ohio2/yjp-yjp/yjp-yjp/yjp99907/yjp8262d07z | xppws | 23:ver.3 | 9/25/09 | 9:22 | Msc: jp-2009-05170u | TEID: brn00 | BATID: 00000

Assessment of the Multiphase Interaction between a Membrane Disrupting Peptide and a Lipid Membrane

Andreea Olaru,[†] Mihaela Gheorghiu,[†] Sorin David,[†] Thorsten Wohland,[‡] and Eugen Gheorghiu*,[†]

International Centre of Biodynamics, Bucharest, Romania, and Department of Chemistry, National University of Singapore, Singapore

Received: June 2, 2009; Revised Manuscript Received: August 28, 2009

Although modeling and experimental approaches to probe antimicrobial peptides−lipid membranes interaction have already been reported, quantitative evaluation of the whole process, including full dissolution of the lipid, is still missing. We report on the real-time assessment of the entire set of stages of melittin−membrane interaction, based on surface plasmon resonance (SPR) measurements, using supported lipid matrices on L1 sensors and long peptide injections. We advance a mathematical model which comprises a set of coupled kinetic equations and relates via the transfer matrix the evolution of lipid and peptide concentrations with the SPR sensorgram. Upon fitting the sensorgrams of melittin injections on POPC lipid matrices, in agreement with literature data, the model provides: association and dissociation rates, concentration thresholds, and evolution within each interacting layer of lipid and peptide concentrations as well as of peptide to lipid ratios. The proposed model combined with appropriate experimental protocols adds new depths to SPR investigation of peptide−lipid interaction offering a quantitative platform for research and controlled design of improved antimicrobial peptides. A wider applicability for quantitative assessment of other pore forming compounds on different lipid matrices is suggested.

Introduction

The ability of antimicrobial peptides (AMP) to lyse pathogen cell membranes offers an attractive solution to the problem of increasing resistance of bacteria to conventional antibiotics.[1] High-resolution techniques provide substantial advances in deciphering the factors influencing the antimicrobial potency.[2] The current view is that the interaction of AMPs with lipid matrices is a complex, multistate process[3,4] consisting of: peptide association to the lipid substrate and its insertion into and destabilization of lipid membranes.

Though several modeling[5,6] and experimental approaches[7−12] were used to probe each step of this interaction, the dynamic assessment of the whole interaction process is still needed.

Aiming for a quantitative description of the complete interaction process between a membrane disrupting peptide (MDP) and a model lipid membrane, we considered comprehensive surface plasmon resonance (SPR) assessment of a lipid modified chip upon continuous injection of a MDP.

Already a standard method in bimolecular analysis, SPR is a powerful tool for high-sensitivity analysis of complex interactions, providing real-time kinetic information on molecular binding and continuous process monitoring.[13] Application of SPR approaches in monitoring peptide−lipid interactions has been reported before.[3,11,14] Among the shortcomings of these studies were the incomplete revelation of the entire process and the rough analysis based on steady state equations or two-stage dynamics.

The objectives of the present work are: (i) to reveal the complete process of peptide−membrane interaction, (ii) to advance a theoretical model comprising a set of the kinetic equations and transfer matrix analysis able to relate the actual concentrations of interacting components to the SPR sensorgram, and (iii) to achieve quantitative analysis of experimental data.

Our approach aims to close the gap between previous studies that emphasize only attachment and insertion of the peptide[11,14,15] and, on the other side, membrane solubilization studies[16−20] dealing with lipid disintegration as a function of peptide concentration.

As a MDP model compound, we chose melittin (MLT) to test the capability of SPR assessment to decipher the multiphase interaction involved in pore formation. A small amphipathic peptide of 26 amino acids, melittin is one of the most widely studied MDPs.[21] It exhibits strong lytic activity against both eukaryotic and prokaryotic cells[22] with mechanisms of interaction depending on the physicochemical properties of the lipid membrane. Charged components[23] and cholesterol[24,25] were shown to have an important impact on the melittin membrane affinity, while the subsequent insertion step is modulated by membrane composition[8] and homogeneity,[25] the peptide/lipid ratio (P/L),[7,26,27] and membrane curvature.[24] The nature of the melittin-induced membrane structural rearrangements, as well as their correlation with membrane leakage, depends on the physical state and composition of the membrane.[24]

Aware of this diversity, the assays were performed on a stable zwitterionic lipid (POPC) matrix formed on top of carboxymethyl dextran surfaces, partially modified with lipophilic, hydrophobic substituents (L1 chip). Notably, the SPR platform can be applied to any kind of lipids or membrane structures with limited modification of the immobilization protocol.

Applying a continuous, long injection of melittin, we reveal for the first time SPR sensorgrams exhibiting the complete set of stages of melittin lipid matrix interaction: melittin attachment and insertion as well as membrane disintegration at various P/Ls

* To whom correspondence should be addressed. Tel.: +40 21 3104354. Fax: +40 21 3104361. E-mail: egheorghiu@biodyn.ro.
[†] International Centre of Biodynamics.
[‡] National University of Singapore.

10.1021/jp905170u CCC: $40.75

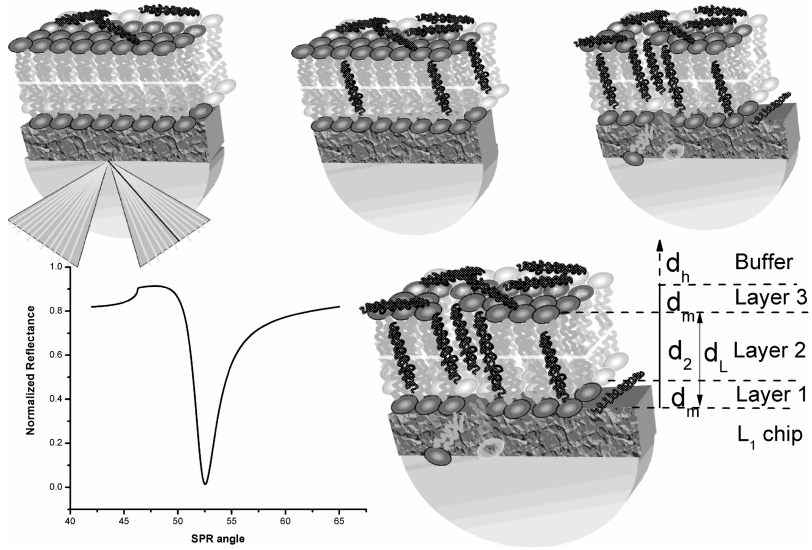

Figure 1. Sketch of the multilayer system corresponding to lipid−melittin interaction and related reflectance spectrum. L1 matrix is represented together with the gold layer. The thicknesses of "evolving" layers are: d_m for Layer 1 and Layer 3 and d_2 for Layer 2; d_h is the height of the buffer.

on a lipid modified L1 chip. To assess the complex behavior related to the entire process of melittin−lipid interaction, we have developed a mathematical model comprising a system of kinetic equations to describe the evolution of lipid and peptide concentrations as well as a procedure, based on transfer matrix analysis, to relate the kinetics to the SPR data. Our approach is applicable to other SPR techniques[12,28] not only to the Biacore assay. A homemade algorithm and the proposed model have been used to fit the experimental data, to derive the concentration thresholds and kinetic parameters for each constitutive phase (association, insertion, and lipid membrane destabilization), and to provide time evolutions of actual P/L within each layer.

Experimental Methods

Materials. Melittin from honey bee venom, CHAPS (3-[(3-cholamidopropyl) dimethyl ammonio]-1-propanesulfonate), HEPES (4-(2-hydroxyethyl) piperazine-1-ethane sulfonic acid), and BSA (bovine serum albumine) were purchased from Sigma-Aldrich (München, Germany), while 1-palmitoil-2-oleyl-sn-glycero-3-phosphocholine (POPC) was from Avanti Lipids (Alabaster, USA). All buffers and reagents were prepared in Milli-Q water. The running buffer was: 10 mM Hepes, 150 mM NaCl, pH 7.4, freshly degassed and 0.22 μm filtered before experiments.

Lipid Vesicles Preparation. Lipid vesicles were prepared (similar to ref 16) by dissolving the POPC lipid in chloroform followed by drying under vacuum in a rotary evaporator for 3 h. The lipid film was hydrated with HEPES buffer and subjected to five sonication cycles, 30 min/cycle. Lipid suspension was extruded 22−25 times using the Mini-extruder (Avanti Lipids, Alabaster, USA) through a 1 μm pore membrane (polycarbonate). Stock solution (1.5 mM) aliquots were stored at +4 °C prior to use.

Lipid Matrix Formation on SPR Biosensor. Biacore 3000 and L1 sensors (Biacore AB, Uppsala, Sweden) were used in all experiments. The L1 sensor surface allows the occurrence of a continuous, stable lipid matrix.

SPR Experiments. The complete SPR assay consists of: (A) L1 sensor surface pretreatment using CHAPS, (B) formation of the lipid membrane, and (C) pore-forming peptide injection. At the end of the experiment, the chip is regenerated using two short injections of CHAPS, 20 mM.

A. Preparation of the Sensor Surface. The sensor chip L1 was installed, normalized,[29] and cleaned by two short (60 s) pulses of CHAPS, 20 μL/min.

B. Formation of the Lipid Membrane. Lipid samples (0.15−0.5 mM concentration, 80 μL) were applied (at 2 μL/min flow rate) to the sensor surface. To remove loosely bound structures and stabilize the baseline, three NaOH 5 min injections (50 mM, 20 μL/min) were applied, rendering stable multilayer lipid matrices. Following BSA injection (10 μL, 0.5 mg/mL, in HEPES buffer), no increase in SPR signal was noticed, indicating full lipid coverage of the L1 surface. The lipid matrix on the chip surface is regarded as a dense multilayer lipid film formed upon liposome adsorption, spreading, and film formation.

C. Peptide Binding to the Lipid Matrix Immobilized on an L1 Chip. Melittin stock solutions were prepared in Milli-Q water at 1 mM final concentration and stored at +4 °C in light protected vials. Spiked melittin samples in HEPES buffer were used at 2.6 μM final test concentration in 65 min injections at 5 μL/min flow rate. All binding experiments were carried out at 25 °C.

Modeling and Data Analyses. In a "classical" SPR experiment,[30] the detected signal (e.g., SPR angle shift) is based on changes in the effective refractive index/dielectric permittivity, considered proportional to the mass accumulated in a single, thin layer at the binding surface.

In contrast, we relate the interaction of melittin with the POPC matrix to a multicompartment system (presented in Figure 1) whose evolving layers shape the overall, "effective" refractive index. Nevertheless, neither a particular structure (e.g., number of individual layers) nor local inhomogeneities (e.g., tightly packed patches) have been considered for the lipid layer. The POPC matrix formed prior to melittin injection is considered to be a homogeneous, planar (multi)layer structure, uniformly covering the L1 surface. This assumption is consistent with recent data that provide theoretical[31] and experimental[32,33] evidence for rupture of adsorbed (zwitterionic) lipid vesicles to form planar supported phospholipid bilayers based on a relatively strong interaction with the substrate surface, appropriate surface charge density, and in appropriate buffer conditions and prior large size liposome accumulation to the surface. Our own optical assays (data not shown) with liposomes loaded with

Rhodamine and Rhodamine−DPPE liposomes are in agreement with ref 33 that indicates, based on AFM and fluorescent approaches on L1 chips, a complete and homogeneous coverage of the surface by phospholipids with no indication of intact liposomes. Furthermore, different thicknesses of the lipid matrix (not individual layers) are considered to account for different SPR signals upon lipid immobilization.

To convert the SPR signal into actual concentrations of the interacting partners, we used the transfer matrix approach in conjunction with a novel multicompartment kinetic model, briefly presented below.

Transfer Matrix. The reflectivity (the fraction of incident field reflected by a surface) is computed based on the transfer matrix method,[34] using repeated application of the Fresnel equation, considering the field distribution, reflection, and transmission within each component of the multilayer system, characterized by the thickness d_i and the complex dielectric constant ε_i. The set of layers is considered to be stacked between a hemispherical prism (Biacore 3000 setup) with dielectric constant ε_p and the semi-infinite medium (running buffer) with dielectric constant ε_h.

P_i and $Q_{i,j+1}$, the propagation and quality matrix, respectively, defined as

$$P_i = \begin{pmatrix} e^{-j\cdot k_{z,i}\cdot d_i} & 0 \\ 0 & e^{j\cdot k_{z,i}\cdot d_i} \end{pmatrix}$$

and

$$Q_{i,i+1} = \frac{1}{2}\cdot\begin{pmatrix} 1+\dfrac{\varepsilon_{i+1}\cdot k_{z,i}}{\varepsilon_i\cdot k_{z,i+1}} & 1-\dfrac{\varepsilon_{i+1}\cdot k_{z,i}}{\varepsilon_i\cdot k_{z,i+1}} \\ 1-\dfrac{\varepsilon_{i+1}\cdot k_{z,i}}{\varepsilon_i\cdot k_{z,i+1}} & 1+\dfrac{\varepsilon_{i+1}\cdot k_{z,i}}{\varepsilon_i\cdot k_{z,i+1}} \end{pmatrix}$$

connect the transmitted and reflected field components within each layer and at the interface between layers, while $k_{z,i} = (\varpi/c)(\varepsilon_i - \varepsilon_p\cdot\sin(\theta)^2)^{1/2}$ are the wave vectors within each layer (corresponding to g, gold; L_1, chip matrix; 1, MLT bound to the L_1 chip; 2, the lipid coating; 3, MLT attached to the lipid; h, running buffer) and θ is the angle of light incidence upon the metal layer. The associated thicknesses are: d_m for the first and third layer and d_2 for the second layer. Melittin assumes different conformations when attached or inserted: above a concentration threshold, it adopts a transmembrane conformation,[35] therefore separate layers related to melittin directly attached to the chip and for the inserted melittin were considered.

The transfer matrix is obtained by multiplication of the matrices **P** and **Q**. Thus, the propagation in every layer and the changes of the field component at the interface to the next layer are taken into account. Within the buffer, the incident field is normalized to 1, and since there is no reflected field, the transfer matrix will be given as:[34]

$$\begin{pmatrix} E_p^+ \\ E_p^- \end{pmatrix} = Q_{p,g}\cdot P_g\cdot Q_{g,L1}\cdot P_{L1}\cdot Q_{L1,1}\cdot P_1\cdot Q_{1,2}\cdot P_2\cdot Q_{2,3}\cdot P_3\cdot Q_{3,h}\cdot\begin{pmatrix}1\\0\end{pmatrix} \quad (1)$$

The transfer matrix combines the entire set of field components and involved layers and can therefore be used to calculate the reflectivity of the complete system provided that thickness and refractive index of all layers, the wavelength, and the angle of incidence θ are given.

To derive the time evolution of the dielectric permittivity of the multilayer system corresponding to the melittin−lipid membrane interaction, we have considered the effective, i.e., equivalent dielectric constant, of each layer in conjunction with the volume concentrations of corresponding compounds. For each layer comprising a mixture of different dielectric media, the equivalence[36] $\varepsilon_{ech} = \Phi_1\cdot\varepsilon_1 + (1-\Phi_1)\cdot\varepsilon_2$ has been used, where Φ_1 is the volume fraction of the compound indexed 1, with the generalized form $\varepsilon_{ech} = \sum_i \Phi_i\cdot\varepsilon_i$. Therefore, we derive the equivalent permittivity of each layer within the system of interest

$$\begin{aligned}
\varepsilon_{ech1} &= \Phi_{l1}[t]\cdot\varepsilon_l + \Phi_{mi1}[t]\cdot\varepsilon_m + \Phi_{ma1}[t]\cdot\varepsilon_m + \\
&\quad (1-\Phi_{ma1}[t]-\Phi_{l1}[t]-\Phi_{mi1}[t])\cdot\varepsilon_h;\\
\varepsilon_{ech2} &= \Phi_{l2}[t]\cdot\varepsilon_l + \Phi_{mi2}[t]\cdot\varepsilon_m + (1-\Phi_{l2}[t]-\Phi_{mi2}[t])\cdot\varepsilon_h;\\
\varepsilon_{ech3} &= \varepsilon_m\Phi_{m3} + \varepsilon_h(1-\Phi_{m3});\\
\varepsilon_{echh} &= \varepsilon_h
\end{aligned} \quad (2)$$

where Φ_{li} is the volume fraction occupied by the lipid in layer i, Φ_{mi} is the volume fraction occupied by the inserted melittin in layer i, with $i = 1, 2$; and Φ_{ma1} and Φ_{m3} are the volume fractions occupied by attached melittin in layer 1 and layer 3, respectively.

The dependency of volume fractions to surface fractions of the respective compounds has been considered within each layer

$$\begin{aligned}
&\Phi_{mi1}[t] = \Phi_{mi2}[t] = S_{mi}[t]/S = \nu_{0i}.m_{ins}[t]\cdot s[t]/S;\\
&\Phi_{l1}[t] = \Phi_{l2}[t] = S_l[t]/S;\\
&\Phi_{l1}[t] = K_l\cdot N_l[t]/(1+\nu_{0i}\cdot m_{ins}[t]\cdot\nu_{om}\cdot m[t])/S;\\
&\Phi_{ma1}[t] = S_{mL1}[t]/S = \nu_{om}\cdot K_m\cdot m_{L1}[t]/S;\\
&\Phi_{m3}[t] = s[t]/S = \nu_{om}\cdot m[t]\cdot S_l[t]/S
\end{aligned} \quad (3)$$

where ν_{0m} is the peptide density; $s[t]$ is the total surface of melittin, with concentration $m[t]$, attached to the lipid (in layer 3); $S_{mi}[t]$ denotes the surface of melittin inserted with concentration $m_{ins}[t]$ within the lipid (layers 1 and 2); $S_l[t]$ is the total surface of lipid, with concentration $N_l[t]$, covering the chip (layers 1 and 2); and $S_{mL1}[t]$ represents the total surface of melittin with concentration $m_{L1}[t]$, attached directly to the surface of the L_1 sensor (layer 1), according to Figure 1.

The equivalent dielectric permittivities, eq 2, have been considered within the transfer matrix to compute the variation in the position of the reflectance minimum (the SPR angle) and compare with the SPR data using a homemade fitting routine.

As Biacore 3000 provides the SPR angle value expressed as relative units, according to ref 30, we use the equivalence: 1 m° SPR angle shift corresponds to 8.2 Relative Units.

Kinetic Model. The interaction of melittin with the lipid matrix formed on the L1 sensor chip is a multiphase, nonmonotonous process[4,14] consisting of several interlinked phases: association, insertion, and destabilization of lipid membrane

On the basis of detailed information, as provided by NMR and oriented circular dichroism (OCD) data,[10,27,37] to describe the entire process we propose a set of kinetic equations, which provides the time evolution of both lipid and melittin concentrations as a function of several threshold concentrations (m_0, m_i, and m_L) and constants: K_{a1} for association, K_{a2} for insertion, and K_{d0} for dissociation of melittin and K_{dl0} for lipid membrane destabilization. We have not taken into consideration the effect of diffusion toward the surface of injected melittin or mass

ohio2/yjp-yjp/yjp-yjp/yjp99907/yjp8262d07z | xppws | 23:ver.3 | 9/25/09 | 9:22 | Msc: jp-2009-05170u | TEID: brn00 | BATID: 00000

transport limitations; the latter are not visible at 5 μL/min flow rate.[38] In the following, we will consider the interaction of melittin with the whole lipid matrix (as a homogeneous structure) and not with each individual layer within. Though a crude approximation of the intricate structure that might be formed on top of the sensor (multilayers or patches of lipids of contrasting densities), this assumption is in line with the actual SPR data that exhibit a smooth dynamics.

• ***Association.*** Melittin in solution attaches to the lipid substrate on the L1 chip in a concentration-dependent manner. Proper sensor coverage with lipids (N_l is the molar concentration of lipids on the surface) provides the putative attachment sites (kN_l) for melittin. This process is reflected by: $K_{a1}N_m(k\cdot N_l[t] - m[t])$, where K_{a1} is the association constant; N_m is the molar concentration of injected melittin; and $m[t]$ is the concentration of the melittin already attached to the lipid matrix at time t.

To assess for the threshold conditions, the Heaviside function of the form

$$H[x] = \begin{cases} 1, x \geq 0 \\ 0, x < 0 \end{cases}$$

has been used within the model.

The association phase determines the build-up of a "layer" of melittin on top of the lipid that influences the subsequent steps: insertion and lipid destabilization. The related equation for melittin reads as

$$m'[t] = K_{a1}N_m(kN_l[t] - m[t])\cdot H[kN_l[t] - m[t]] - K_{d0}kN_l[t]/N_{l0}\cdot m[t]\cdot H[N_l[t]] - k_{ai}\cdot m'_{ins}[t] \quad (4)$$

Moreover, we assume coupled phases; i.e., insertion starts whenever a threshold concentration of the attached peptide is reached, corresponding to a given P/L, in agreement with Zemel[39] and in contrast to the model proposed by Papo[11] that considers parallel processes. The constant k_{ai} relates the rate of association to the one of insertion.

• ***Insertion.*** Evolution of melittin concentration inserted into the lipid matrix m_{ins} is prompted by $m[t]$ reaching a threshold value m_0,[39] and since the attached melittin is the source for insertion, it is considered to depend on the excess of attached melittin $m[t]$ above m_0. Insertion cannot progress indefinitely, therefore a threshold value corresponding to the maximum concentration of inserted melittin, m_i (dependent on the lipid amount on the surface), has been proposed. To account for melittin-induced lipid dissociation, weighted thresholds (m_0 and m_i) by the ratio between the actual and the lipid concentration prior to melittin injection, $N_l[t]/N_{l0}$, are considered. The rate of insertion is set by K_{a2}, corresponding to the fully inserted (whole lipid height) melittin concentration. This simplification that neglects the actual progression of insertion along the lipid depth is motivated by an appropriate balance between the complexity of the model and the dimensionality of SPR data.

Accordingly, the equation for insertion is given by

$$m'_{ins}[t] = K_{a2}\left(m[t] - m_0\frac{N_l[t]}{N_{l0}}\right)\cdot\left(m_i\frac{N_l[t]}{N_{l0}} - m_{ins}[t]\right)\cdot H\left[m[t] - m_0\frac{N_l[t]}{N_{l0}}\right]\cdot H\left[m_i\frac{N_l[t]}{N_{l0}} - m_{ins}[t]\right] \quad (5)$$

•***Dissociation of Lipid Matrix (Membrane Destabilization).*** Melittin attachment and insertion affect the lipid matrix leading to its destabilization. Whether "carpet" like or "pore formation",[27,40] the recent models of interaction provide clear indication of threshold values triggering matrix disintegration of either attached or inserted melittin. Corresponding to these particular cases, two terms have been considered in the equation for the rate of lipid dissociation: (a) one assessing the effect of attached melittin, dependent on the dissociation constants K_{dL0} and the difference between the attached $m[t]$ and the threshold m_L, triggering lipid dissociation, and (b) the other one corresponding to the effect of inserted melittin, dependent on dissociation constants K_{dL0ins} and the difference between the inserted $m_{ins}[t]$ and the threshold $m_{Lins,}$ triggering lipid dissociation.

Thus, the related terms

$$K_{dl0}N_l[t]\left(m[t] - m_L\frac{N_l[t]}{N_{l0}}\right)\cdot H[N_l[t]]\cdot H\left[m[t] - m_L\frac{N_l[t]}{N_{l0}}\right]$$

and

$$K_{dl0ins}N_l[t]\left(m_{ins}[t] - m_{L_{ins}}\frac{N_l[t]}{N_{l0}}\right)\cdot H[N_l[t]]\cdot H\left[m_{ins}[t] - m_{L_{ins}}\frac{N_l[t]}{N_{l0}}\right]$$

have been evaluated against the measured data. Since our experiments corresponding to injections of peptide in the high-concentration domain were consistent with a dominant effect of attached melittin (first term) compared with the inserted one (second term), in the analysis of respective data, the simplified form is used

$$N'_l[t] = -K_{dl0}\frac{N_l[t]}{N_{l0}}\left(m[t] - m_L\frac{N_l[t]}{N_{l0}}\right)\cdot H[N_l[t]]\cdot H\left[m[t] - m_L\frac{N_l[t]}{N_{l0}}\right] \quad (6A)$$

For the particular case of intermediate melittin concentration (e.g., 2.35 μM), the data are consistent with a prevailing effect of inserted melittin on lipid dissociation (as inferred by the toroidal model[26]), and the second term is dominant and therefore is used for fitting the corresponding data.

$$N'_l[t] = -K_{dl0ins}N_l[t]\left(m_{ins}[t] - m_{L_{ins}}\frac{N_l[t]}{N_{l0}}\right)\cdot H[N_l[t]]\cdot H\left[m_{ins}[t] - m_{L_{ins}}\frac{N_l[t]}{N_{l0}}\right] \quad (6B)$$

This dissociation phase generates lipid "voids" and progressive uncoverage of the sensor chip. Preliminary tests of direct binding of mellitin on the unmodified L1 chip show significant attachment (~1000 RU for 3.3 μM, data not shown). To assess for this adsorption process, we have introduced eq 7

$$m'_{L1}[t] = K_{a3}N_m(RR - N_l[t]/N_{l0})\cdot(N_{CO} - m_{L1}[t])\cdot H[RR - N_l[t]/N_{l0}]\cdot H[N_{CO} - m_{L1}[t]] \quad (7)$$

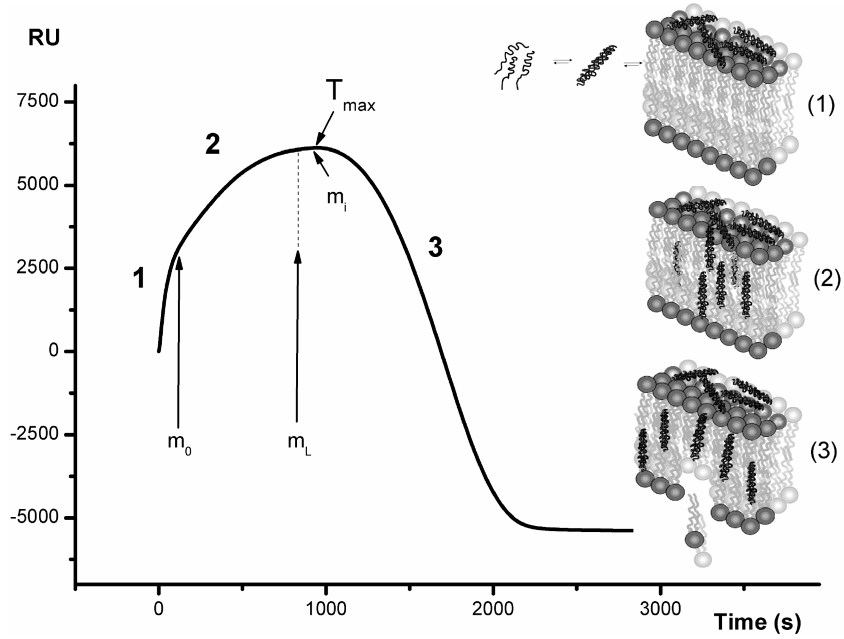

Figure 2. Multiphase interaction between melittin and a lipid membrane immobilized on the L1 sensor as revealed by SPR data: (1) melittin attachment, (2) melittin attachment and insertion, (3) melittin attachment, insertion, and lipid destabilization. The arrows indicate the positions corresponding to T_{max}, when the maximum SPR signal is reached and the time points when the threshold concentrations for initiation of insertion, m_0, and lipid dissociation, m_L, are attained, as well as m_i, the threshold limiting peptide insertion.

TABLE 1: Notations Used within the Mathematical Model

notations used within the mathematical model	
	concentrations [M]
$m[t]$	melittin concentration bound at time t on the surface of lipid matrix
$m_{ins}[t]$	melittin concentration inserted into the lipid matrix
$m_{L1}[t]$	melittin concentration bound directly to the sensor surface
N_m	melittin concentration injected continuously during the experiment
$N_l[t]$	lipid concentration at time t
N_{C0}	concentration of melittin binding sites on the sensor surface
m_0	threshold concentration for the beginning of the insertion process
m_i	threshold concentration when the insertion process ends
m_L	threshold concentration of attached melittin when the lipid membrane starts to disintegrate
m_{Lins}	threshold concentration of inserted melittin when the lipid membrane starts to disintegrate
	association constants [$M^{-1}s^{-1}$]
K_{a1}	for the melittin association process onto the lipid membrane
K_{a2}	for the insertion process
K_{a3}	for the peptide attachment on the sensor surface
	dissociation constants [s^{-1}]
K_{dl0}	lipid dissociation constant, due to attached melittin
K_{dl0ins}	lipid dissociation constant, due to inserted melittin
K_{d0}	melittin dissociation constant
	other notations
$H[x]$	heaviside function; $H[x] = 1$, $x \geq 0$, and $H[x] = 0$, $x < 0$.
RR	threshold value corresponding to lipid sensor uncoverage to enable melittin attachment directly to the chip
N_{C0}	concentration of the binding sites for melittin on the L1 chip
k_{ai}	parameter relating the rate of association to the one of insertion
k	parameter related to the actual melittin binding sites on lipid unit

corresponding to the evolution of melittin attached directly to the L1 chip ($m_{L1}[t]$ as a function of the binding sites N_{C0}, injected melittin concentration, and the association rate K_{a3} as a measure of melittin "affinity" for the L1 chip; the degree of lipid uncoverage to determine direct attachment is defined as: $RR - N_l[t]$.

To solve (numerically) the equations, initial conditions were imposed: $m[0] = m_{00}$; $m_{ins}[0] = 0$; $N_l[0] = N_{l0}$; $m_{L1}[0] = 0$. A summary of the parameters within the kinetic model is listed in Table 1.

Data Analysis. Due to the structure of the kinetic equations (comprising terms accounting for thresholds) and the inherent complexity of the SPR response of the evolving layers involved in MDP−membrane interaction, no analytical solution exists. The alternative has been to work out a numerical computation approach (comprising integration of kinetic equations, assessment of transfer matrices of the multicompartment model, and nonlinear data fitting) able to provide access to the evolution

of concentrations of interacting components as well as to the respective kinetic constants and thresholds. Sequential analysis of the coupled equations, as the dynamics of the interaction process is continuously assessed, limits the number of fitted parameters in each round of analysis and controls the apparent large dimension of the model (11 model parameters are determined).

The calculations, including data analysis and curve fitting, were performed with Mathematica (version 6.0, Wolfram Research Europe Ltd., UK). Whenever applicable, comparisons were performed with BIA evaluation software (Biacore, Sweden) and WinSpal (version 3.01, http://www.mpip-mainz.mpg.de/knoll/soft/).

Results

SPR Sensorgrams of the Complete Interaction Process, Including Lipid Dissociation. Using a continuous, 65 min injection of melittin in the micromolar range, we reveal, for the first time, the complete interaction process, from melittin association until lipid dissolution. The SPR level corresponding to the lipid coverage of the L1 chip is considered the "reference level" for melittin injection, thus all experimental sensorgrams are normalized to 0 at the beginning of peptide injection.

According to a representative sensorgram (Figure 2), the SPR data reveal all the interlinked phases associated with the general model of interaction of MDP with lipids and considered in our specific kinetic model (eqs 5−8) association, insertion, and lipid membrane destabilization. A characteristic feature is the occurrence of T_{max}, the time point when the SPR signal reaches a maximum value before lipid destabilization.

Qualitative Analysis of Experimental Sensorgrams and Data Normalization. Following lipid immobilization, the SPR signal is dependent on the concentration of the lipids in the liposome solution and on the quality of the surface of the L_1 chip. Low immobilization thresholds, ~3000 RU, have been obtained (data not shown) for 0.05 mM concentration of lipids. Typical experimental data considered in our analysis have SPR responses for the immobilized lipid matrix in the range of 6100−8800 RU. Using extensive calibrations on L_1 chips (data not shown), transfer matrix approach, and the characteristic volume of the POPC lipid unit, 1.32 nm,[3,41] the lipid matrix thickness and related volume concentration were evaluated and fed into the fitting procedure. Different concentrations of 1 μm size vesicles provide lipid matrices with thickness in the range of 14−20 nm (based on 1.45 value for the refractive index of the lipid layer).

The representative SPR signals at different P/L presented Figure 3A show significant variability in the measured values. Yet, the proposed normalization procedure, eq 8, involving the amplitude and time of the peak value in the sensorgram, reveals a similar behavior corresponding to a general interaction process independent of the lipid immobilization level (Figure 3B).

$$(RU_{ech} - RU_f)/(RU_{echmax} - RU_f) = f(t/t_{max}) \qquad (8)$$

Analysis Flowchart. To derive the model parameters (comprised in eq 4−7) from the experimental data, we have developed a homemade fitting routine with the following landmarks:

1. Numerical integration of the coupled differential equations to derive time evolution of the volume concentrations of each component.

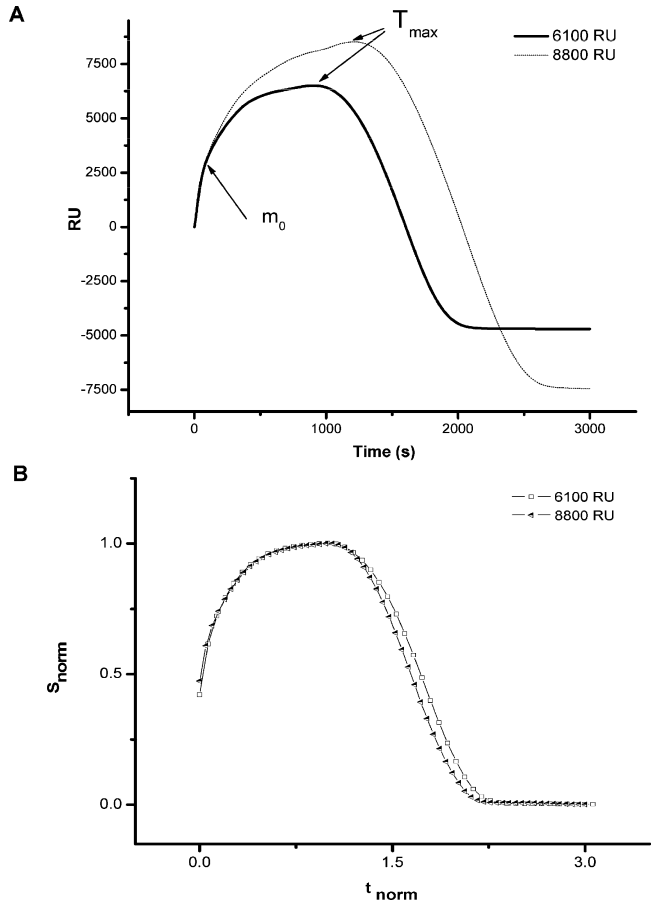

Figure 3. Experimental and normalized SPR sensorgrams for melittin injections (2.6×10^{-6} M) performed for ~1 h. The lipid membrane immobilization levels vary between 6100 and 8800 RU. Normalized signals $S_{norm} = (RU_{ech} - RU_f)/(RU_{echmax} - RU_f)$ versus $t_{norm} = t/T_{max}$ for the experimental data.

2. Relate volume concentrations to corresponding volume fractions in the distinct layers (Figure 1) and compute the effective permittivity ε_{eff1}, ε_{eff2}, ε_{eff3}, of the layers with thickness d_m, d_2, and d_m, respectively.

3. Derive the SPR angle based on the application of the transfer matrix on the multilayer system. To check for consistency, we used WinSpal 3.01 software.

As the measured SPR signal, in relative units, is directly related to the SPR angle shift derived from the application of the transfer matrix, the fitting routine provides the parameters of the model.

On the basis of our modeling approach, Figure 4 shows the dependency of the SPR angle on different compositions of the multilayer system on top of the L1 sensor. In the inset, the related time points and actual RU values in an experimental sensorgram are given.

Fitting Parameters. The set of model parameters and their values derived by fitting the experimental sensorgrams, comprises:

1. Parameters independent of the thickness of the lipid film, indicated in Table 2A;

2. Parameters dependent on the thickness of the lipid film, indicated in Table 2B;

3. Geometrical and material parameters having the same value for different experimental conditions (i.e., different lipid coverage and amount of injected melittin) in Table 2C .

A typical sensorgram for the peptide interaction with an artificial lipid membrane immobilized on the L1 sensor chip is

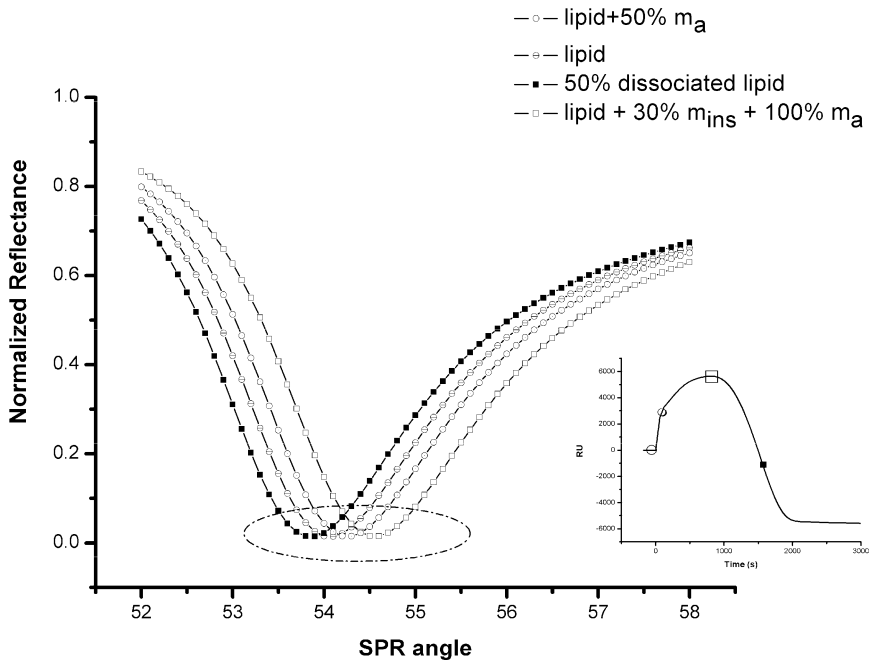

Figure 4. SPR spectra as a function of the actual composition in each evolving layer of the peptide−lipid complex: θ, modified lipid sensor; ○, melittin attached; □, melittin attached and inserted ■ upon lipid dissociation. In the inset: the corresponding time points in a typical sensorgram in relation to the SPR dip position.

F5 presented in Figure 5A. The derived values of parameters K_{a1}, K_{a2}, K_{d0}, m_0, m_i, m_L, K_l, K_m, k_{ai}, K_{dl0}, K_{a3}, RR, N_{C0}, and k are given in the figure caption.

Figure 5B reveals the time evolution of the concentrations of melittin attached and inserted and the concentration of lipid on the sensor chip as derived using the kinetic model. The corresponding time evolutions of the actual molar P/L in each interacting layer are derived for the first time from SPR data (Figure 5C).

Time evolutions of the absolute amounts of inserted ($Q_{mins}[t]$) and attached ($Q_{matt}[t]$) peptide derived based on eq 9 are presented in Figure 5D, following extensive calibration experiments (data not shown) to circumvent the lack of data on the actual L_1 chip parameters (e.g., density, refractive index, height of the dextran matrix).

$$\begin{aligned} \rho_m &= \frac{m[t]\cdot S_l[t]\cdot MW_m}{s[t]} \\ Q_{m_{att}}[t] &= s[t]\cdot d_m\cdot \rho_m \\ Q_{m_{ins}}[t] &= S_i[t]\cdot d_L\cdot \rho_m \end{aligned} \qquad (9)$$

where MW_m and ρ_m are the molecular weight (2846 Da) and density of melittin, respectively.

F6 Figure 6 shows the predicted SPR sensorgrams for different lipid levels for a constant peptide concentration based on the model and a representative set of parameters to simulate an extended set of lipid coverage conditions. The related dependencies of the estimated T_{max} as a function of lipid coverage are analyzed against the corresponding experimental data (error bars).

The derived values for the parameters of the kinetic model are presented in Table 2A, while the input parameters are presented in Table 2B.

Discussion

Monitoring the Whole Process of Interaction between Melittin and a Lipid Matrix. Monitoring peptide−lipid interactions by SPR assays has been reported before[3,11,14] recommending the technique as a powerful tool for investigating real-time interactions between membrane disrupting compounds and lipid matrices. Previous SPR studies have used either small (<0.37 μM) or extremely large (90 μM) peptide concentrations and limited injection times (6−16 min), insufficient to reveal the whole process of peptide−lipid interaction, including lipid dissociation.

In contrast, during one hour injection of melittin (1.6−3.6 μM), we reveal for the first time SPR sensorgrams exhibiting the complete melittin−lipid matrix interaction, including melittin attachment and insertion and membrane solubilization (Figures 1 and 3A), at various P/L. Our approach, on a lipid modified L1 chip, closes the gap between previous studies on model membranes[11,14,15] that emphasize only attachment and insertion of the peptide and membrane solubilization studies[16−20] dealing with lipid disintegration as a function of peptide concentration.

Although the lipid film consists of a multilayer structure, since the SPR sensorgrams do not reveal any abrupt changes that should have corresponded to a layer-by-layer dissociation of the lipid matrix or to the passage of inserted melittin from one layer to the subsequent one, our simplified model assumes a homogeneous structure of the lipid membrane.

On the basis of a planar lipid matrix configuration, the same concentration of melittin conceivably leads to the same threshold concentration for the attached peptide to initiate insertion, the lipid amount influencing the dynamics of the insertion step. Higher lipid coverage is associated with longer interaction times until lipid dissociation is initiated (occurrence of a peak value, T_{max}, in the sensorgram). Once initiated, lipid dissociation progresses with similar pace (comparable downward slopes in the dissociation phase) toward SPR levels corresponding to the ones before lipid immobilization.

ohio2/yjp-yjp/yjp-yjp/yjp99907/yjp8262d07z | xppws | 23:ver.3 | 9/25/09 | 9:23 | Msc: jp-2009-05170u | TEID: brn00 | BATID: 00000

TABLE 2: Derived Kinetic Parameters for Injections of the Same Concentration (2.6 μM) of Melittin (A) Independent and (B) Dependent of the Thickness of Lipid Films and (C) Numerical Values for the Geometrical and Material Parameters Considered in the Fit

(A) mean values for kinetic parameters independent of the thickness of lipid film

step of the multiphasic process	related parameters	estimated
association	K_{a1} ($\times 10^3$ M^{-1} s^{-1})	2.13 ± 0.52
	K_{d0} ($\times 10^{-4}$ s^{-1})	4.35 ± 4.19
insertion	m_0 ($\times 10^{-2}$ M)	2.40 ± 0.01
	normalized m_i (M/lipid bilayer)	0.0292 ± 0.0005
peptide attachment on sensor surface	K_{a3} ($\times 10^4$ M^{-1} s^{-1})	1.51 ± 0.11
	RR	0.17 ± 0.03

(B) kinetic parameters dependent on the thickness of the lipid film

	thickness of the lipid film		
	14 nm	16 nm	20.2 nm
insertion		K_{a2} ($\times 10^{-2}$ M^{-1} s^{-1})	
	4.41 ± 0.05	4.29 ± 0.05	1.72 ± 0.06
		m_i (M)	
	0.135 ± 0.006	0.153 ± 0.003	0.236 ± 0.004
membrane destabilization		K_{dl0} (s^{-1})	
	0.059 ± 0.004	0.041 ± 0.006	0.018 ± 0.005
		m_L (M)	
	0.179 ± 0.002	0.181 ± 0.003	0.297 ± 0.003

(C) numerical values for the geometrical and material parameters considered in the fit

notation	description	value
d_L	$d_2 + d_m$ = lipid matrix thickness	$14 \pm 20.1 \times 10^{-9}$ (m)
d_m	thickness of attached melittin layer	$8.8 \pm 2.5 \times 10^{-9}$ (m)
S	flow channel total surface	1.2×10^{-6} (m^2)[29,49]
$n_i = \varepsilon_i^{1/2}$	refractive index and permittivity value; i = l,h,m	
n_l	lipid refraction index	1.45[9,50]
n_h	buffer refraction index	1.3315[51]
n_m	melittin refraction index	1.675[51]
v_{0m}	molar volume of associated melittin	2.68 ± 0.15 (M^{-1})[51,52]
v_{0i}	molar volume of inserted melittin	2.76 ± 2.11 (M^{-1})
N_{l0}	concentration of lipid on the chip prior to melittin injection	1.26 ± 0.01 (M)
N_{C0}	concentration of melittin binding sites on L1 chip	5.23 ± 0.13 ($\times 10^{-6}$ M)
K_l	coefficient denoting surface coverage per lipid molar concentration	9.5×10^{-7} (m^2 M^{-1})
K_m	coefficient denoting surface coverage of 1 mol melittin attached to the L1 chip	10^{-2} (m^2)
k_{ai}	parameter relating the rate of association to the one of insertion.	0.72 ± 0.13
k	parameter related to the actual melittin binding sites on a lipid unit	0.196 ± 0.055

The proposed normalization procedure, eq 8, reveals this pattern of interaction (Figure 3B), independent of the lipid immobilization level.

Kinetic Model of Peptide−Lipid Interaction. The proposed model, consisting of eqs 2−7, provides the kinetic characterization of the complete interaction process between melittin and lipid membranes based on numerical analysis of SPR data.

Previous attempts to derive kinetic models exist;[11,14,15] however, the proposed equations, two-state or parallel reaction models, involve equilibrium values of the overall SPR signal, without any reference to the dynamics of interacting partners. Alternatively, we relate the SPR sensorgram to the evolution of interacting compounds within the "evolving" layers on the chip.

The numerical computation comprising integration of kinetic equations, assessment of transfer matrices of the multicompartment model, and nonlinear data fitting is able to provide access to the evolution of interacting components concentration as well as to the respective kinetic constants and thresholds.

The set of kinetic equations has been designed in compliance with the present mechanistic knowledge. As described in eq 4, with increasing peptide binding, upon reaching a threshold, melittin begins to insert into the membrane and undergoes reorientation.[27]

Transmembrane conformation assumed that once the melittin inserts it is reflected in the different pace of insertion and associated kinetic constant (K_{a2}) revealed by lipid matrices with different thicknesses. One should note the scarcity of available data for comparison: most of the lipid kinetic data or threshold values have not been previously derived, while literature data for K_{a1} are available only for DMPG/DMPC[14] or mixed layers of PC/cholesterol and PE/PG[11] not suitable for direct comparison. Nevertheless, the derived values, such as K_{a1}, K_{d0}, K_m, and K_{a2} and m_0, were checked against the ones provided by control experiments: low melittin concentration revealing only association and or insertion and shorter peptide injections followed by comprehensive injection of buffer provided direct assessment of the dissociation processes (data not shown) and were found in perfect agreement.

Although we consider the insertion of melittin as a process affecting the complete stack within the lipid structure, not individual layers, m_i values derived from fit are linearly dependent on the amount of lipid on the chip (correspondingly on the thickness of the lipid film). m_i normalization to the

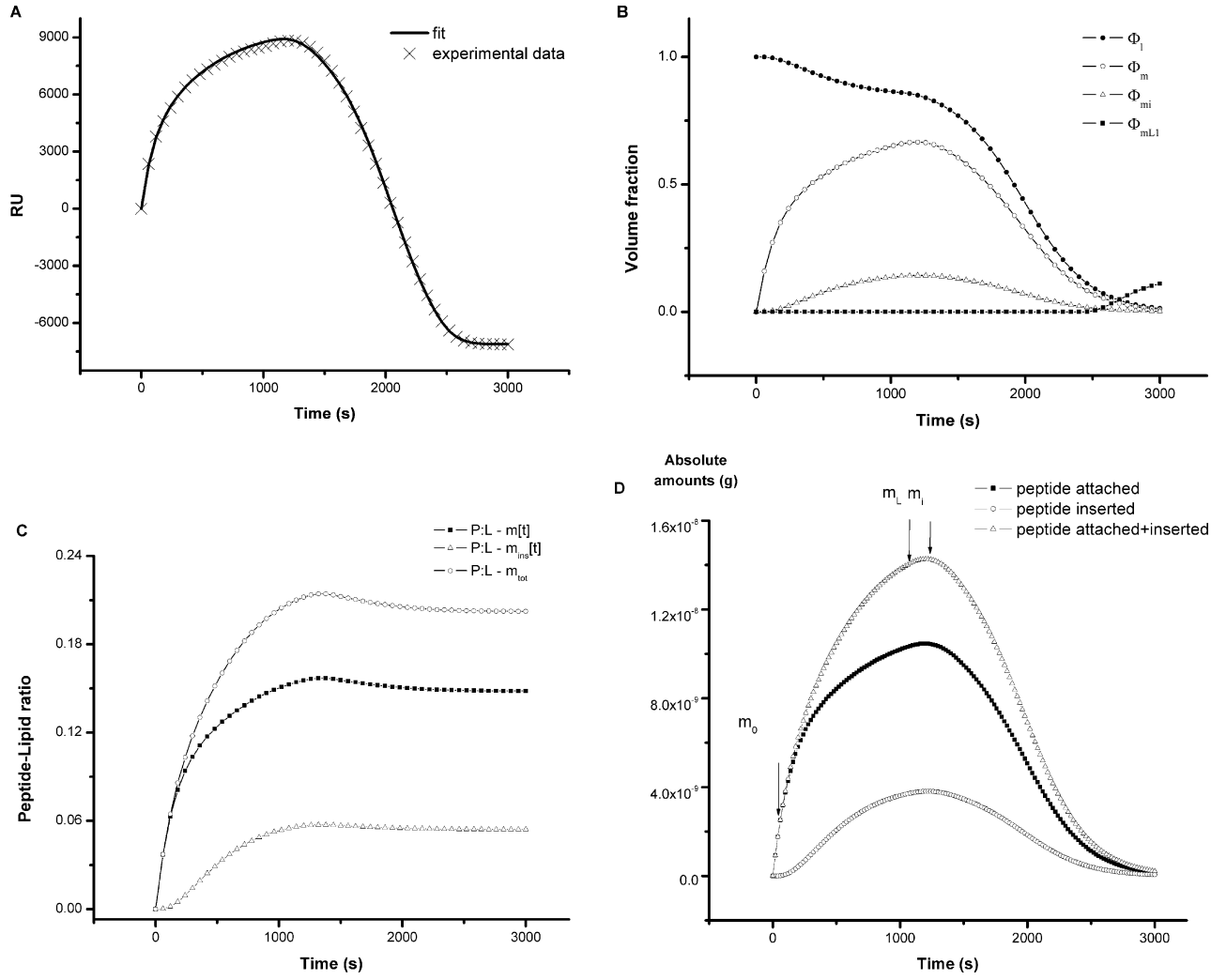

Figure 5. Time evolution of SPR data and of selected model parameters corresponding to peptide−lipid interaction. (A) Typical sensorgram with the corresponding fit of melittin (concentration 2.6 μM, ∼1 h injection time) and lipid matrix (immobilization level 8800 RU). Fitting kinetic parameters are given in Table 2A and 2B (column corresponding to 20.2 nm), whereas the geometric and material ones are given in Table 2C. (B) Lipid matrix and the related volume fractions of melittin associated to the lipid and directly to the L_1 matrix, inserted in the lipid matrix (●, volume fractions of lipid in layers 1 and 2; ○, volume fraction of melittin attached to the lipid, layer 3; Δ, volume fraction of melittin inserted in layer 2; ■, volume fraction of melittin attached directly to the L1 chip, layer 1). (C) Time evolution of the peptide/lipid ratios corresponding to associated $m[t]$ ■, inserted $m_{ins}[t]$ Δ, and total $m_{tot}[t]$ ○ melittin concentrations for the same lipid coverage of 8800 RU. (D) Time evolution of the amounts of attached ■, inserted ○, and total (attached and inserted) Δ melittin for the same lipid coverage of 8800 RU. Also indicated are the time points when the threshold concentrations for initiation of insertion, m_0, of lipid dissociation, m_L, and m_i limiting peptide insertion are attained.

estimated number of layers within the whole thickness of the lipid (each layer is considered to have 3 nm thickness) provides a nearly constant 0.0290 ± 0.0005 M concentration per bilayer for the different lipid films involved in our analysis.

As melittin is injected as well during the lipid dissociation step, we consider a direct melittin binding to the uncovered L1 chip as an additional process during the dissociation phase. This binding process, and not remaining lipid coverage, may account for the residual signal of ∼1400 RU, especially since CHAPS pulses that completely remove the lipid from the surface are less efficient in regenerating melittin (data not shown).

Relevance of the Kinetic Model. The set of coupled differential equations provides the dynamics for each of the components within the multilayer system which are related via the transfer matrix to the SPR angle corresponding to the actual SPR data (Figure 4). As such, the model allows a sufficient degree of flexibility with no a priori consideration of a molecular model of interaction.

Despite the vast literature available (for a recent review see ref 24), assessment of the interaction between AMPs and lipid membranes in respect to a clear mechanism of action is still under scrutiny. Yet, the formation of transmembrane pores in the target cell is suggested by most of the studies[6] as a compelling mechanism. Membrane partition can be completed either by pore formation via a "barrel-stave" mechanism or by a membrane solubilization (detergent-like) "carpet" mechanism. Both mechanisms depend on the peptide charge and the mode of self-association in the target membrane.[4,42] Nevertheless, the latter gains more and more support from experimental and molecular dynamics simulation data[5,6,26] as the general model of interaction of antimicrobial peptides with lipid membranes.

On the basis of the attachment and insertion equations 4 and 5, we derive kinetic and threshold values revealing their dependence on the concentration of injected melittin and membrane affinity. Moreover, the lipid dissociation equation, eq 6A, 6B, is not considered in any reported study aimed to provide insight on the interaction model and peptide efficiency in destabilizing the lipid matrix. As revealed by data analysis, lipid dissociation is largely dependent on randomly associated/

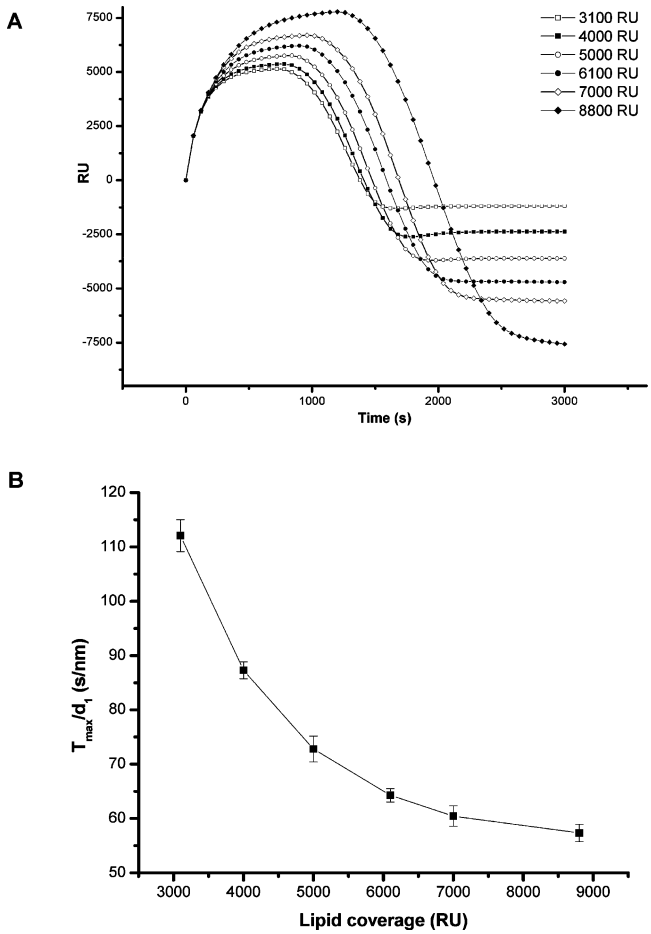

Figure 6. (A) SPR simulated curves for different lipid coverages: □, 3100 RU; ■, 4000 RU; ○, 5000 RU; ●, 6100 RU; ◇, 7000 RU; and ♦, 8800 RU, for a 2.6 μM peptide concentration. (B) Dependence of the ratio: T_{max}/thickness of lipid matrix on the SPR signal corresponding to the lipid coverage and the standard deviations from the experimental ones.

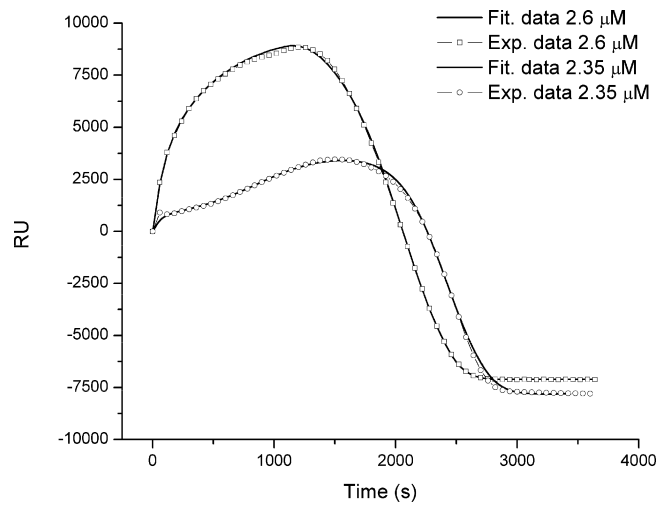

Figure 7. Experimental sensorgrams revealing different apparent association constants and correspondingly different kinetics for different injected peptide concentrations (2.35 and 2.6 μM) and the respective fits. The lipid coverage is similar: 8600 and 8800 RU, respectively. Fitted kinetic parameters for 2.35 μM are: $K_{a1} \sim 1.084 \times 10^3$ M^{-1} s^{-1}; $K_{a2} \sim 6.32 \times 10^{-2}$ M^{-1} s^{-1}; $K_{a3} \sim 1.64 \times 10^4$ M^{-1} s^{-1}; $K_{d0} \sim 3.9 \times 10^{-4}$ s^{-1}, $K_{dl0ins} \sim 0.021$ s^{-1}; $RR \sim 0.14$; $m_0 \sim 0.024$ M; $m_i \sim 0.308$ M; $m_{Lins} \sim 0.307$ M. The geometric and material ones are given in Table 2C; for 2.60 μM, the fitted parameters are the same as given in Figure 5A.

inserted melittin, with no defined pore structure. This makes our results consistent with "carpet-like"/"toroidal pore" models.

L1 regeneration conditions are not fully optimized.[43,44] Therefore, assessment of mellitin attachment directly to the chip (as described by eq 7) in relation to different regeneration conditions could support improvement of the experimental protocol toward sensing applications.

Quantitative Description of SPR Data. Fitting the experimental data (Figure 5A), the model provides kinetic parameters and time evolutions of concentrations of melittin, attached and inserted, and of the lipid, suitable to be compared with data reported in the literature. Representative evolutions of the derived surface coverage and volume fractions are presented in Figures 5B and 5C.

Most of the literature reports rely on the use of liposomes to derive kinetic data on peptide−lipid interactions. In general, P/L is used as a quantitative measure of the experimental conditions, while specific markers are deployed to assess the degree of membrane permeability/fluidity. For neutral lipids, low melittin concentrations induce pore formation with pore size depending on the melittin concentration. For anionic and/or nonbilayer forming lipids, melittin induces fusion or aggregation of liposomes accompanied by a specific leakage.[45]

On the other hand, supported lipid (bi)layers are less studied, with a handful of different approaches based on OCD,[8] dual polarization interferometry,[12,28,46] and SPR among the most prominent ones.

According to ref 27, OCD and neutron scattering experiments on multilayers of lipids on solid supports reveal that in POPC membranes there is 85% of melittin oriented parallel to the membrane ("attached") for a P/L of 1/40, while 68% of melittin is oriented transversal ("inserted") to the membrane for a P/L of 1/15.

According to our data, the threshold of insertion, m_0, corresponds, in the case of 8800 RU lipid coverage, to a P/L equal to 1/44. The fast kinetics of the association phase (the threshold value is attained in ~20 s) is determined only by the concentration of injected melittin (note the small standard deviation for K_{a1} derived for three different lipid coverages and the same concentration of melittin, Table 2A). As the injected melittin concentration is in the micromolar range and we used salt supplemented HEPES buffer pH 7.4, possible oligomerization of melittin in solution[38,47] could influence the association constant K_{a1} ($1.46 \pm 0.11 \times 10^3$ M^{-1}, for a lower concentration range, data not shown). The slightly higher value derived for K_{a1} compared with refs 11 and 14 should as well be interpreted based on the different lipid composition and concentration range used.

Besides evolution of the actual P/L ratios, the model provides time series of the absolute amounts of inserted and attached peptide as presented in Figure 5D.

Notably, the derived density of melittin, given by eq 9, is lower than the value from the literature (1.41 g cm^{-3})[52] by ~20%, highlighting the reliability of our approach.

The dynamics revealed by the SPR signal is highly dependent on the balance between the kinetics of melittin association and insertion. The rates of these processes are modulated by the surface concentration of melittin, which is in turn determined by the concentration of injected melittin.

Experimental evidence of this situation is presented in Figure 7 where two different concentrations of melittin, 2.35 versus 2.6 μM, have been injected over sensors with similar lipid coverage (8600 and 8800 RU, respectively). Lower concentration of injected melittin determines in the initial association

phase (the first 100 s) a slightly lower pace; upon reaching the insertion threshold, this smaller association rate versus the insertion one leads to subsequent attenuation of the overall kinetics. Even though the association constant K_{a1} is lower, melittin attachment and insertion progresses and eventually determines total lipid dissolution. In contrast to the data for high concentration of melittin where lipid dissociation is largely dependent on the attached melittin (eq 6A), the fitting procedure in the case of 2.35 μM was done using lipid dissociation dependency related to the inserted peptide (eq 6B). The cases where both contributions (attachment and insertion of melittin) are effective for lipid dissociation are to be considered in a different study.

Our observations are in agreement with those based on Sum Frequency Generation Vibrational Spectroscopy analysis where it is suggested[26] that melittin functions via the early (only association) and late stage of the carpet model (lipid destabilization) at low (below 0.5 μM) and high concentrations (above 3 μM), respectively, whereas the toroidal model seems adequate at intermediate concentrations.

The quantitative analysis of the experimental data on a lipid coverage corresponding to 8800 RU provides distinct volume fractions as melittin insertion progresses leading to gradual lipid destabilization and finally to lipid dissociation. At around 300 s, 12% of the whole melittin is inserted corresponding to a 2/17 total P/L. According to Figure 5C, the P/L corresponding to initiation of lipid dissociation is 2/13 for the attached melittin and 1/5 for the total melittin concentration. We emphasize the similitude with the reported values for V4 synthetic peptide[17] where membrane disruption occurs as well at a ratio V4/lipid $\sim$1/4 for POPG liposomes.

On the basis of the threshold concentrations, i.e., m_0 and m_i for the insertion stage and m_l for the lipid membrane disintegration and the moment of their occurrence, one can achieve a quantitative assessment of the process of peptide−lipid interaction and can compare the effect of different peptides and/or lipid compositions. In particular, the interaction of newly synthesized peptides or modified native antimicrobial peptides[48] to achieve better specificity against microbial infections with the lowest side effect on the host organism can be quantitatively assessed. In view of simplifications encompassed by our model, the appraisal of other systems should involve amendments of both kinetic equations and transfer matrix approach in agreement with both experimental sensorgrams and support data concerning the interacting partners.

T_{m0} (the time when m_0 threshold occurs) can be conveniently used for rapid quantification of the concentration of injected melittin as well as for comparing the affinities of the different peptides to the same or different lipid matrices, as is mainly governed by the affinity constant and the injected peptide concentration.

T_{mi} (the time when m_i threshold occurs) reveals a clear dependence on the amount of lipid on the surface and can be used to compare different experimental conditions.

We used our model to simulate an extended set of lipid coverage conditions. Figure 6A shows the predicted SPR sensorgrams for different lipid levels, while the peptide concentration is maintained constant. Figure 6B reveals the related dependencies of the estimated T_{max} as a function of lipid coverage.

Conclusions

Using the advantages offered by SPR, i.e., label-free, real-time monitoring of analyte−ligand interaction, this study reveals the complex, multiphasic interaction mechanism between melittin, a model MDP, and a model lipid matrix provided by POPC. Similar behavior/dynamics corresponding to a common, general interaction process, independent of the thickness of the lipid matrix, have been revealed by handling the experimental data according to a normalization procedure. The distinct, yet interlinked phases (association, insertion, and lipid membrane disruption) are described by fitting the experimental data with the proposed kinetic model.

As a novelty, our approach relates the evolution of interacting compounds assessed by the kinetic model to the "evolving" layers on the chip that are further integrated in the transfer matrix to derive the corresponding SPR response.

Quantitative evaluation of the complete SPR sensorgram provided by numerical analysis based on our model offers direct insight into representative, effective kinetic parameters and time evolutions of lipid and melittin concentrations during the specific phases of the entire process.

Besides the capability to properly fit the experimental data, our model is able to provide relevant information on time evolution of "hidden" parameters, i.e., lipid and melittin concentration and their volume fractions. The actual P/L are derived for each step encompassed by melittin−lipid interaction closing the gap between the reported literature values, concerning experiments in solution, to the ones on solid supports.

The proposed model combined with appropriate experimental protocols adds a new depth to the classic SPR investigation of peptide−lipid interaction offering a quantitative platform for understanding the manifold facets of the interaction and for supporting the controlled design of new, improved antimicrobial peptides. Having in view the similar interaction patterns reported[16] for virus mimetic attack, we stress on a wider applicability of our approach for quantitative assessment of the effect of other pore-forming compounds on different lipid membranes, thus on a broader biophysical significance.

Acknowledgment. Support of the EU NMP3-SL-2008-214107 Nanomagma project as well as the support of Eastern Europe Research Scientists and Students Exchange & Collaboration Programme (EERSS) of the National University of Singapore is acknowledged.

References and Notes

(1) Hancock, R. E.; Sahl, H. G. *Nat. Biotechnol.* **2006**, *24*, 1551.
(2) Brogden, K. A. *Nat. Rev. Microbiol.* **2005**, *3*, 238.
(3) Mozsolits, H.; Wirth, H. J.; Werkmeister, J.; Aguilar, M. I. *Biochim. Biophys. Acta* **2001**, *1512*, 64.
(4) Shai, Y. *Biochim. Biophys. Acta* **1999**, *1462*, 55.
(5) Leontiadou, H.; Mark, A. E.; Marrink, S. J. *J. Am. Chem. Soc.* **2006**, *128*, 12156.
(6) Marrink, S. J.; de Vries, A. H.; Tieleman, D. P. *Biochim. Biophys. Acta* **2009**, *1788*, 149.
(7) Bastos, M.; Bai, G.; Gomes, P.; Andreu, D.; Goormaghtigh, E.; Prieto, M. *Biophys. J.* **2008**, *94*, 2128.
(8) Constantinescu, I.; Lafleur, M. *Biochim. Biophys. Acta* **2004**, *1667*, 26.
(9) Frey, S.; Tamm, L. K. *Biophys. J.* **1991**, *60*, 922.
(10) Naito, A.; Nagao, T.; Norisada, K.; Mizuno, T.; Tuzi, S.; Saito, H. *Biophys. J.* **2000**, *78*, 2405.
(11) Papo, N.; Shai, Y. *Biochemistry* **2003**, *42*, 458.
(12) Popplewell, J. F.; Swann, M. J.; Freeman, N. J.; McDonnell, C.; Ford, R. C. *Biochim. Biophys. Acta* **2007**, *1768*, 13.
(13) Besenicar, M.; Macek, P.; Lakey, J. H.; Anderluh, G. *Chem. Phys. Lipids* **2006**, *141*, 169.
(14) Lee, T. H.; Mozsolits, H.; Aguilar, M. I. *J. Pept. Res.* **2001**, *58*, 464.
(15) Mozsolits, H.; Thomas, W. G.; Aguilar, M. I. *J. Pept. Sci.* **2003**, *9*, 77.
(16) Chah, S.; Zare, R. N. *Phys. Chem. Chem. Phys.* **2008**, *10*, 3203.

(17) Yu, L.; Guo, L.; Ding, J. L.; Ho, B.; Feng, S. S.; Popplewell, J.; Swann, M.; Wohland, T. *Biochim. Biophys. Acta* **2009**, *1788*, 333.
(18) Pott, T.; Paternostre, M.; Dufourc, E. J. *Eur. Biophys. J.* **1998**, *27*, 237.
(19) Pott, T.; Dufourc, E. J. *Biophys. J.* **1995**, *68*, 965.
(20) Maulet, Y.; Brodbeck, U.; Fulpius, B. *Biochim. Biophys. Acta* **1984**, *778*, 594.
(21) Dempsey, C. E. *Biochim. Biophys. Acta* **1990**, 1031.
(22) Asthana, N.; Yadav, S. P.; Ghosh, J. K. *J. Biol. Chem.* **2004**, *279*, 55042.
(23) Stromstedt, A. A.; Wessman, P.; Ringstad, L.; Edwards, K.; Malmsten, M. *J. Colloid Interface Sci.* **2007**, *311*, 59.
(24) Lundquist, A.; Wessman, P.; Rennie, A. R.; Edwards, K. *Biochim. Biophys. Acta* **2008**, *1778*, 2210.
(25) Wessman, P.; Stromstedt, A. A.; Malmsten, M.; Edwards, K. *Biophys. J.* **2008**, *95*, 4324.
(26) Chen, X.; Wang, J.; Kristalyn, C. B.; Chen, Z. *Biophys. J.* **2007**, *93*, 866.
(27) Yang, L.; Harroun, T. A.; Weiss, T. M.; Ding, L.; Huang, H. W. *Biophys. J.* **2001**, *81*, 1475.
(28) Mashaghi, A.; Swann, M.; Popplewell, J.; Textor, M.; Reimhult, E. *Anal. Chem.* **2008**, *80*, 3666.
(29) *Biacore 3000 Instrument Handbook*; Biacore AB: Sweden, 2003.
(30) *Handbook of Surface Plasmon Resonance*; Schasfoort, B. M. R., Tudos, J.A., Eds.; RSC Publishing: Cambridge U.K., 2008.
(31) Morigaki, K.; Tawa, K. *Biophys. J.* **2006**, *91*, 1380.
(32) Cha, T.; Guo, A.; Zhu, X.-Y. *Biophys. J.* **2006**, *90*, 1270.
(33) Erb, E.-M.; Chen, X.; Allen, S.; Roberts, C. J.; Tendler, S. J. B.; Davies, M. C.; Forsén, S. *Anal. Biochem.* **2000**, *280*, 29.
(34) Born, M.; Wolf, E. *Principles of optics: electromagnetic theory of propagation, interference and diffraction of light*, 6th ed.; Pergamon Press: Oxford; New York, 1980.
(35) Gaidukov, L.; Fish, A.; Mor, A. *Biochemistry* **2003**, *42*, 12866.
(36) Peterlinz, K. A.; Georgiadis, R. *Langmuir* **1996**, *12*, 4731.
(37) Ladokhin, A. S.; White, S. H. *Biochim. Biophys. Acta* **2001**, *1514*, 253.
(38) Henriques, S. T.; Pattenden, L. K.; Aguilar, M. I.; Castanho, M. A. *Biophys. J.* **2008**, *95*, 1877.
(39) Zemel, A.; Ben-Shaul, A.; May, S. *Eur. Biophys. J.* **2005**, *34*, 230.
(40) Allende, D.; Simon, S. A.; McIntosh, T. J. *Biophys. J.* **2005**, *88*, 1828.
(41) Pinisetty, D.; Moldovan, D.; Devireddy, R. *Ann. Biomed. Eng.* **2006**, *34*, 1442.
(42) Oren, Z.; Shai, Y. *Biopolymers* **1998**, *47*, 451.
(43) Nakajima, H.; Kiyokawa, N.; Katagiri, Y. U.; Taguchi, T.; Suzuki, T.; Sekino, T.; Mimori, K.; Ebata, T.; Saito, M.; Nakao, H.; Takeda, T.; Fujimoto, J. *J. Biol. Chem.* **2001**, *276*, 42915.
(44) Baird, C. L.; Courtenay, E. S.; Myszka, D. G. *Anal. Biochem.* **2002**, *310*, 93.
(45) van den Bogaart, G.; Mika, J. T.; Krasnikov, V.; Poolman, B. *Biophys. J.* **2007**, *93*, 154.
(46) Terry, C. J.; Popplewell, J. F.; Swann, M. J.; Freeman, N. J.; Fernig, D. G. *Biosens. Bioelectron.* **2006**, *22*, 627.
(47) Vogel, H.; Jahnig, F. *Biophys. J.* **1986**, *50*, 573.
(48) Kim, H. K.; Lee, D. G.; Park, Y.; Kim, H. N.; Choi, B. H.; Choi, C. H.; Hahm, K. S. *Biotechnol. Lett.* **2002**, *24*, 347.
(49) Malmqvist, M.; Roos, A. K. H.; Sjolander, S.; Tidare, M.; Sjodin, A. K. H.; Ang St., L. R. Method and device for laminar flow on a sensing surface Biacore AB (Uppsala, SE) 2001; Vol. United States Patent 6200814
(50) Anderluh, G.; Besenicar, M.; Kladnik, A.; Lakey, J. H.; Macek, P. *Anal. Biochem.* **2005**, *344*, 43.
(51) Voros, J. *Biophys. J.* **2004**, *87*, 553.
(52) Terwilliger, T. C.; Weissman, L.; Eisenberg, D. *Biophys. J.* **1982**, *37*, 353.

JP905170U